

# Quality Versus Sparsity in Image Recovery by Dictionary Learning Using Iterative Shrinkage

1<sup>st</sup> Mohammadsadegh Khoshghaferezaee

*Institute for Mathematics*

*Brandenburg University of Technology*

Cottbus, Germany

khoshmoh@b-tu.de

2<sup>nd</sup> Moritz Krauth

*Institute for Mathematics*

*Brandenburg University of Technology*

Cottbus, Germany

krautmor@b-tu.de

3<sup>rd</sup> Shima Shabani

*Institute for Mathematics*

*Brandenburg University of Technology*

Cottbus, Germany

shima.shabani@b-tu.de

4<sup>th</sup> Michael Breuß

*Institute for Mathematics*

*Brandenburg University of Technology*

Cottbus, Germany

breuss@b-tu.de

**Abstract**—Sparse dictionary learning (SDL) is a fundamental technique that is useful for many image processing tasks. As an example we consider here image recovery, where SDL can be cast as a nonsmooth optimization problem. For this kind of problems, iterative shrinkage methods represent a powerful class of algorithms that are subject of ongoing research. Sparsity is an important property of the learned solutions, as exactly the sparsity enables efficient further processing or storage. The sparsity implies that a recovered image is determined as a combination of a number of dictionary elements that is as low as possible. Therefore, the question arises, to which degree sparsity should be enforced in SDL in order to not compromise recovery quality. In this paper we focus on the sparsity of solutions that can be obtained using a variety of optimization methods. It turns out that there are different sparsity regimes depending on the method in use. Furthermore, we illustrate that high sparsity does in general not compromise recovery quality, even if the recovered image is quite different from the learning database.

**Index Terms**—sparse dictionary learning, image recovery, basis pursuit denoising, nonsmooth optimization, iterative shrinkage

## I. INTRODUCTION

To process signals or images, it is considered useful to have models that represent the data. The sparse model offers a particularly effective method, exploiting inherent sparsity and redundancy of signal representations [3]. It proposes that for a class of signals  $\Gamma \subset \mathbb{R}^m$ , a redundant dictionary  $D \in \mathbb{R}^{m \times n}$  ( $n \gg m$ ) exists composed of  $n$  prototype signals or atoms. The core assumption is that any signal in  $\Gamma$  can be accurately represented by a sparse linear combination of such atoms. Redundancy, meaning that the dictionary's dimensionality exceeds that of the data, facilitates highly sparse representations.

Learning the dictionary from training data rather than relying on pre-defined bases (e.g., wavelets) is a way to emphasize the sparse representation of training signals drawn from  $\Gamma$  and

We acknowledge funding by the German Aerospace Center (DLR) as part of project AIMS: Artificial Intelligence Meets Space, grant no. 50WK2270F, and by the Bundesministerium für Bildung und Forschung (BMBF) within the project KI@MINT ("AI-Lab").

is called *sparse dictionary learning* (SDL). Methods of SDL have been used e.g. for Poisson denoising [9], in clustering [11], or deblurring [23].

Turning to SDL optimization, corresponding methods concurrently optimize for an adapted dictionary and its associated sparse representations. This can be formulated as a matrix decomposition problem, in which the training data matrix is approximated as the product of a dictionary matrix and a sparse representation matrix. The solution is obtained through iterative minimization, typically involving alternating phases of *dictionary updating* and *sparse coding*. The implementation of these stages varies across different SDL algorithms [3]. The question arises, how sensitive high representation quality is with respect to the degree of sparsity enforcement and if this is influenced by the choice of the SDL method. A potentially related issue is, if there is in addition to the obvious sparsity parameter an aspect in the SDL setup that has a large influence on the sparsity property.

In this paper we consider the class of iterative shrinkage methods, which represent a powerful tool for SDL optimization. Even though building upon the same concept and solving the same optimization problem, we show that the sparsity of results from different methods may differ in general. We show that there are typical sparsity regimes that do not seem to compromise recovery quality, even generalizing beyond a small set of training images. In addition, we demonstrate that atom dimension has a substantial influence on sparsity.

## II. RELATED WORK

Considering SDL optimization methods, let us briefly mention some of the main developments. The Method of Optimal Directions (MOD) [5] focuses on minimizing the representation error while constraining the number of non-zero coefficients in the sparse representation. A probabilistic approach has been proposed in [14] building upon independent component analysis and singular value decomposition (SVD).

Another approach [13] makes use of a block coordinate relaxation algorithm [18] for sparse coding and SVD for atom updates. The K-SVD method [1] also utilizes SVD for atom updates and enforces sparsity similar to MOD.

A more flexible setting is presented in terms of an online SDL algorithm in [15], facilitating especially to learn based on numerous small patches extracted individually from given imagery. Employing the online SDL framework, [21] studies the impact of training dataset on dictionary construction and recovery quality, providing some insights into method selection and parameter tuning. However, [21] does not consider the sparsity property and related aspects of the setup.

As a perspective conceptually related to the focus of the current paper, one may consider dictionary learning as a variation of sparse matrix factorization [3]. Similarly as in our work, in such matrix factorization problems the sparsity of matrices is directly of interest. Since corresponding models may allow the extraction of interpretable patterns from multiway data, there is significant research in developing algorithms that perform constrained low-rank matrix approximations [7], [24]. However, unlike in typical matrix factorization problems, we specifically deal here with SDL for image recovery.

### III. SPARSE DICTIONARY LEARNING

Traditional dictionary learning methods [1], [17] formulate the learning problem as minimizing the reconstruction error on a training dataset  $\Gamma \equiv \{p_i\}_{i=1}^N$ , with  $p_i \in \mathbb{R}^m$  expressed as:

$$\min_{D, x_i} \sum_{i=1}^N \|Dx_i - p_i\|_2^2 \quad \text{w.r.t.} \quad \|x_i\|_0 \leq T \quad (1)$$

Here,  $T$  limits the number of non-zero elements in the sparse representation  $x_i \in \mathbb{R}^n$ , effectively controlling sparsity. The goal is to simultaneously determine the dictionary  $D$  and the corresponding sparse representations  $x_i$  for the training samples.

Although the  $\ell_0$  norm ( $\|\cdot\|_0$ ) intuitively captures the notion of sparsity by counting non-zero entries, it poses challenges for practical optimization. Therefore, a common approach is to approximate the non-convex  $\|\cdot\|_0$  norm with a convex surrogate. Specifically, in the sparse coding stage, techniques like those in [15]  $\ell_1$  norm ( $\|\cdot\|_1$ ) instead, resulting in the following optimization problem:

$$\min_{D, x_i} \frac{1}{N} \sum_{i=1}^N \left( \frac{1}{2} \|Dx_i - p_i\|_2^2 + \mu \|x_i\|_1 \right) \quad (2)$$

where parameter  $\mu$  specifically controls sparsity. Let us emphasize, that the  $\ell_1$  penalty still encourages sparse solutions as explained geometrically in [3]. The optimization problem (2) exhibits convexity concerning each variable when the other is constant. This allows for an alternating minimization strategy, iteratively optimizing for one variable while fixing the other.

Concerning interpretation of computational results, let us note that we constrain the Euclidean norm of the dictionary atoms. So, in (2), we restrict  $D$  to a convex set  $\mathcal{C}$  defined as,  $j = 1, \dots, n$ :

$$\mathcal{C} = \left\{ D = [d_1, \dots, d_n] \in \mathbb{R}^{m \times n} \mid d_j \in \mathbb{R}^m, d_j^T d_j \leq 1 \right\} \quad (3)$$

#### A. Standard Sparse Recovery Methods

With a fixed dictionary  $D$ , the sparse recovery stage in (2) becomes a convex  $\ell_2$ - $\ell_1$  optimization problem, commonly known as *basis pursuit denoising*:

$$\min_x \frac{1}{2} \|Dx - p\|_2^2 + \mu \|x\|_1 \quad (4)$$

In this paper, we consider a variety of classical and recent shrinkage-thresholding methods such as FPC-BB [10], TwIST [2], GSCG [6], ISGA [19], and smISGA [20]; see e.g. [21] for some more details on these methods.

---

#### Algorithm 1: Dictionary Learning

---

**Data:**  $D_0 \in \mathbb{R}^{m \times n}$  (initial dictionary),  $\Gamma$  (patch set),  
 $p \in \mathbb{R}^m$  (image patch),  $N$  (number of the patches),  
 $\mu \in \mathbb{R}$  (regularization parameter)

**Result:**  $D_N$  (learned dictionary)

```

1 List = {FPC - BB, TwIST, GSCG, ISGA, smISGA}
2 Select a solver from the List;
3  $A_0 \leftarrow 0$ ,  $B_0 \leftarrow 0$  (reset the past information);
4 for  $k = 1$  to  $N$  do
5   Draw  $p_k$  from  $\Gamma$ ;
6   Sparse Coding Stage:
7      $x_k = \arg \min_{x \in \mathbb{R}^n} \frac{1}{2} \|D_{k-1}x - p_k\|_2^2 + \mu \|x\|_1;$ 
8      $A_k \leftarrow A_{k-1} + x_k x_k^T$ ;
9      $B_k \leftarrow B_{k-1} + p_k x_k^T$ ;
9   Dictionary Updating Stage: Update  $D_k$  using
10  Algorithm 2 with  $D_{k-1}$  as a warm restart, so that
11    
$$D_k = \arg \min_{D \in \mathcal{C}} \frac{1}{k} \sum_{i=1}^k \frac{1}{2} \|Dx_i - p_i\|_2^2 + \mu \|x_i\|_1$$

12    
$$= \arg \min_{D \in \mathcal{C}} \frac{1}{k} \left( \frac{1}{2} \text{Tr}(D^T D A_k) - \text{Tr}(D^T B_k) \right)$$

10 end

```

---

#### B. Online Dictionary Learning Algorithm

Leveraging the online SDL approach outlined in [15], [21], we investigate the influence of different sparse recovery techniques. Algorithm 1 summarizes the SDL methodologies. The algorithm begins by selecting a specific sparse coding solver, which dictates the dictionary learning strategy (lines 1-2). In each iteration, a random patch is extracted from the training dataset  $\Gamma$  (line 5). The core of the algorithm (lines 4-10) comprises two essential phases: sparse coding (lines 6) and dictionary atom updating (line 9). To maintain the independence of each iteration, the algorithm resets the accumulated information related to the sparse coefficients computed for previous patches (lines 7-8). This necessitates an initialization step (line 3) to prepare the data structures. In sparse coding stage at iteration  $k$ , with the dictionary  $D_{k-1}$  from the previous iteration held constant, line 6 calculates

---

**Algorithm 2:** Dictionary Updating

---

**Data:**  $D_{k-1} \in \mathbb{R}^{m \times n}$ ,  
 $A_k = [a_1, \dots, a_n] = \sum_{i=1}^k x_k x_k^T \in \mathbb{R}^{n \times n}$ ,  
 $B_k = [b_1, \dots, b_n] = \sum_{i=1}^k p_k x_k^T \in \mathbb{R}^{m \times n}$ .

**Result:**  $D_k$

```

1 while convergence do
2   for  $j = 1$  to  $n$  do
3     Update the  $j$ -th column to optimize for (5)
4
5   end
6 end

```

---

the sparse representation of the selected patch  $p_k$  using the chosen sparse coding solver. In the dictionary updating stage in Algorithm 2 by block coordinate descent method at iteration  $k$ , the algorithm leverages  $D_{k-1}$  as a warm start, incorporating the accumulated and fixed sparse representation of all patches up to that point in  $A_k$  and  $B_k$ . Updates are performed selectively on atoms with non-zero sparse coding contributions ( $A_{jj} \neq 0$ ). It is column-wise, updating one atom at a time while adhering to the constraint  $d_j^T d_j \leq 1$ .

#### IV. EXPERIMENTS

Let us first elaborate on the experimental setting. The experiments were conducted in MATLAB R2024b on an egino BTO system. To evaluate dictionaries, we considered a colorful random subset of 100 images of resolution  $224 \times 224$  of the Kaggle data set [12]. We did some preprocessing to make them ready for the learning.

First, we convert them to grayscale and then to a double-precision array. If not stated otherwise, we extracted 15000 random patches as with stride 2 or 75% overlapping and size  $8 \times 8$  from the random selected images. Let us note that subsequently, the patch size and correspondingly the degree of overlapping may vary. 75% overlapping means each patch has 75% of its area in common with the adjacent patches. So, the process extracts 11881 patches from each image. Then, patch-wise dictionary learning has been done over 15000 random patches, constituting our  $\Gamma$  set, i.e.,  $N = 15000$  in Algorithm 1. Based on the patch size ( $8 \times 8$ ), the size of the produced redundant dictionaries is  $64 \times 256$ .

Concerning underlying computational options, the initial dictionary  $D_0 \in \mathbb{R}^{64 \times 256}$  is determined by employing a discrete cosine transform, the result of which is normalized. As initial values for sparse recovery we consider  $x_0 = \mathbf{0}_{256 \times 1}$ .

The stopping condition for all solvers in line 6 of Algorithm 1 is given by

$$\|x_{k+1} - x_k\|_2 \leq \epsilon_1 \|x_k\|_2 \quad (7)$$

with  $\epsilon_1 = 10^{-7}$  for GSCG, ISGA, and smISGA and  $\epsilon_1 = 10^{-5}$  for FPC-BB and TwIST or if the number of iterations exceeds 5000000. For image reconstruction with learned dictionaries in terms of the original image ( $\text{Img}_{\text{org}}$ ) and reconstructed image ( $\text{Img}_{\text{rec}}$ ), the stopping criterion is as

$$\|\text{Img}_{\text{org}} - \text{Img}_{\text{rec}}\|_F \leq \epsilon_2 \|\text{Img}_{\text{org}}\|_F \quad (8)$$

using the Frobenius norm, with  $\epsilon_2 = 10^{-10}$  for GSCG, ISGA, and smISGA and  $\epsilon_2 = 10^{-5}$  for FPC-BB, and TwIST, or if the number of iterations exceeds 5000000. The differences in setting  $\epsilon_1$  and  $\epsilon_2$  are necessary to achieve results of comparable reconstruction quality, see [21] for related discussion. All other parameters of any given solver are the default as described in the corresponding paper.

Turning to quantitative error measures, we measure the relative error  $\text{RelErr}$  between original and reconstructed images (relative w.r.t. the original image) in the Frobenius norm, as well as the absolute of the maximum deviation  $\text{Dev}$  between original and reconstruction. Let us note that for these measures, all images are given in terms of standard grey-scale range [0, 255], where reconstructed images are not quantized in tonal domain to integer format. Furthermore, we consider the structural similarity index  $\text{SSIM}$  which is a perceptual metric in contrast the aforementioned error measures.

#### A. Experiment 1: Sparsity vs. Reconstruction Quality

We now briefly explore if the described SDL approach gives high quality results for image recovery in terms of standard error measures. In order to assess quality for different degrees of sparsity, we let the sparsity parameter  $\mu$  vary over different orders of magnitude by setting  $\mu = 2^{-8}, 2^{-4}, 2^{-1}$  in the optimization problem (4). Let us note that  $\mu = 2^{-8}$  appears to be a standard choice in compressed sensing [6], [10], [19], [20]. However, in compressed sensing the underlying problem dimensions are often much larger than in the current work.



Fig. 1. Test images from Kaggle dataset employed in first two experiments.

Results given in Table I are averaged over our set of test set of six images displayed in Figure 1. The numbers in Table I show that even at medium-size sparsity coefficient  $\mu = 2^{-4}$ , some of the methods give a virtually exact result, as a deviation of less than 0.5 grey scale units is supposedly not visible at all.

TABLE I  
RECONSTRUCTION QUALITY MEASURES, AVERAGED OVER OUR TEST DATASET

Tested Algorithms	Sparsity Coefficient								
	2 <sup>-8</sup>			2 <sup>-4</sup>			2 <sup>-1</sup>		
	RelErr	Dev	SSIM	RelErr	Dev	SSIM	RelErr	Dev	SSIM
FPC-BB	0.00005	0.03	1.000	0.0006	0.30	0.999	0.0039	2.01	0.999
TwIST	0.00016	0.06	1.000	0.00055	0.28	1.000	0.0049	2.13	0.999
GSCG	0.00004	0.02	1.000	0.0006	0.30	0.999	0.0042	2.17	0.999
ISGA	0.00115	1.32	0.999	0.0059	6.35	0.999	0.0178	11.23	0.994
smISGA	0.00078	1.07	0.999	0.0031	1.86	0.999	0.0106	6.40	0.998

The computationally much more efficient methods ISGA and smISGA admit single points of higher deviations, yet the low relative error indicates that only a small set of pixels is affected at all. The higher range of sparsity coefficient  $\mu = 2^{-1}$  means that sparsity is emphasized over accuracy, so all methods show some deviations in these measures. While deviations of few grey levels in just some pixels as indicated in the table still represent visually convincing reconstructions. This is also the reason why we do not display recovered results here, as they are virtually identical to our test images.

In total, even a higher regime of sparsity parameters  $\mu$  does not compromise recovery quality significantly. In turn, the actual degree of sparsity may remain hidden when assessing just quality measures of recovery results.

### B. Experiment 2: Sparsity Assessment

We now consider the sparsity of coefficients in the setting of the first experiment, i.e. for  $\mu = 2^{-8}, 2^{-4}, 2^{-1}$  in optimization problem (4). For sparsity assessment, we employ a binning of the values of the reconstruction coefficients using 100 bins. In this way we obtain histograms of coefficient values. The desirable sparsity property means that a significant peak should be observable for the bins at or around zero, since this would indicate that a corresponding majority of coefficients do not contribute significant image information.

The main observations of this experiment are summarized at hand of Figure 3. As observable, the default histogram shape appears to be a Gaussian. This is intuitively not surprising, given that in optimization problem (2) the data fidelity term is modeled by employing the  $\ell_2$  norm, inducing a Gaussian statistics of coefficients. The role of the sparsity constraint is to extract and diminish from that Gaussian distribution of coefficients the ones that do not hinder reconstruction.

In total, we observe three main sparsity regimes that occur at some stage depending on the optimization method. We conjecture that the results differ depending on the obtained minimization paths for the different methods.

While the low regime of  $\mu$  values yields a Gaussian distribution of coefficients with no visible impact of the sparsity constraint, already the medium regime of  $\mu$  values results in significant portion of diminished coefficients for some of the methods, namely FPC-BB, TwIST and GSCG. This is visible at hand of a clear peak, within a Gaussian-type distribution of other coefficients. For ISGA and its refined version smISGA

even higher regimes of  $\mu$  values are necessary to obtain such highly sparse solutions. Let us note that, when comparing the widths of the Gaussian part of distributions for all methods and any values of  $\mu$ , there is no apparent contraction towards zero, meaning that the overall shape is preserved apart from the peak. In highly sparse regime, the peak is highly tweaked and dominates the Gaussian-type distribution of other coefficients.

As supplementary experiment, we consider reconstructions of second test image when thresholding the peak values, see Figure 2. Plotting the remaining histogram, we clearly see the Gaussian distribution of remaining coefficients. Furthermore, the reconstruction is highly accurate at all tested regimes so that only a significant scaling of differences enables to get a visual impression at all. This observation at hand of Figure 2 is quantitatively confirmed by the SSIM measures in Table I.

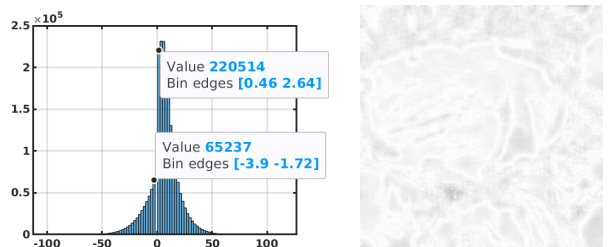


Fig. 2. Histogram after removing peak and corresponding difference images (inverted and scaled by factor 50 for visualization) FPC-BB in (displayed with peak in first row, second column of Fig. 3).

### C. Experiment 3: Influence of Patch Size

In this experiment we aim to analyze the influence of the patch size respectively the atom size in our SDL setup. Let us note that the total computational setting is of not too high dimensions. For subsequent experiments, our dictionaries are fixed to 512 atoms to properly deal with different patch sizes. The number of rows in turn are given by the atom dimension determined by the patch size. Larger patch sizes also result in higher degree of overlap when keeping the stride 2 fixed as in this experiment. We combine this experiment by testing at the same time for generalization capability. While the dictionary is learned via Kaggle dataset, we now reconstruct the classical Barbara test image.

For quantitative evaluation, we propose to fit a Gaussian distribution curve to the arising histograms of coefficients and

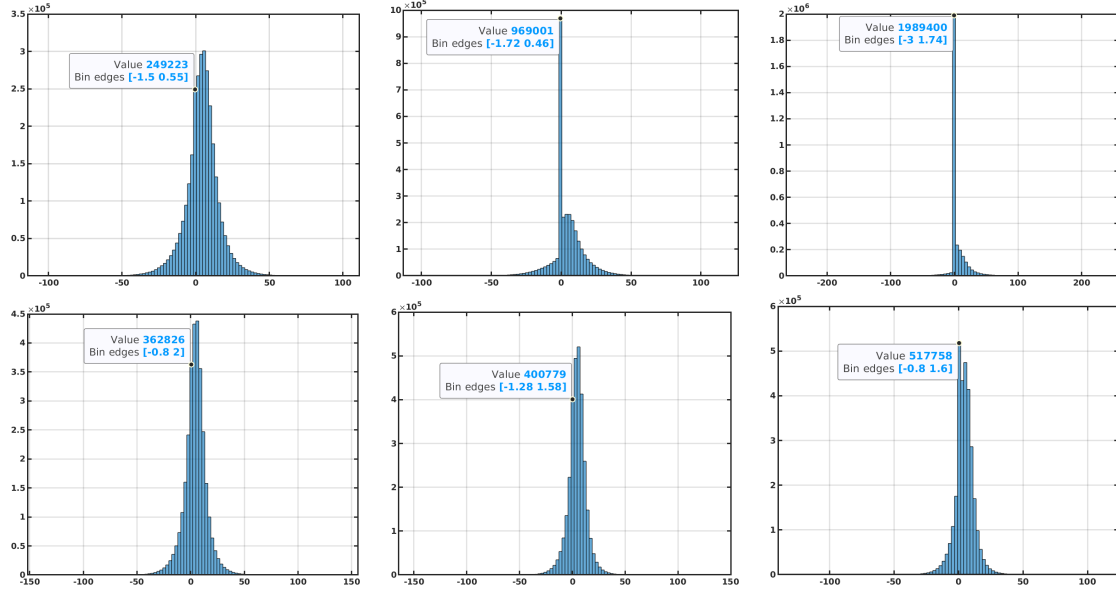


Fig. 3. Sparsity comparison among FPC-BB, and ISGA (rows) with  $\mu = 2^{-8}, 2^{-4}, 2^{-1}$  (columns) for second test image. The results for TWIST and smISGA are similar to FPC-BB and ISGA, respectively. The results of GSCG are in between FPC-BB and ISGA. For obtaining similar results showcasing a peak as in the first row with ISGA and smISGA, we have to employ values such as  $\mu = 2^1, 2^2$ . The information in the boxes show the number of values in the peak and the corresponding bin edges around zero.

focus especially on the standard deviations of the Gaussians, as these give a clear indication of the sparsity fitness. In addition, we also consider the previous quality measures.

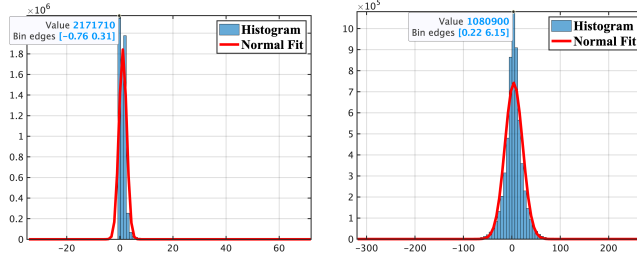


Fig. 4. Histogram with Gaussian fit for FPC-BB method with patch sizes  $4 \times 4$  and  $14 \times 14$ , respectively.

As confirmed by subsequent Tables II and III (mean and standard deviation by  $m$  and  $\sigma$ , respectively), increasing the patch size may lead to a certain loss of quality, but especially the sparsity is degraded. The difference between the two tested algorithms ISGA and FPC-BB is here, that the ISGA method is for  $\mu = 2^{-4}$  still in the regime of low sparsity and features a clear, unperturbed Gaussian distribution of coefficients. In this regime, the impact of increasing patch size is quite severe in both quality and Gaussian distribution parameters. The FPC-BB method is for  $\mu = 2^{-4}$  in the sparsity regime featuring a clear peak of diminished coefficients. In this sparsity regime we do not observe a significant degradation of quality, but the underlying Gaussian distribution of coefficients as well as the sparsity is clearly affected by increasing patch sizes.

In total, parameter selection in the regime of clearly ob-

TABLE II  
ATOMS=512,  $\mu = 2^{-4}$ , STRIDE=2. EVALUATION OF QUALITY: RELATIVE ERROR, DEVIATION, AND SSIM FOR BARBARA TEST IMAGE ( $224 \times 224$ )

Patch	Tested algorithms					
	ISGA			FPC-BB		
	RelErr	Dev	SSIM	RelErr	Dev	SSIM
4x4	0.0003	0.291	1.00	0.0001	0.204	1.00
8x8	0.0099	10.73	0.99	0.0004	0.522	0.99
14x14	0.0394	43.67	0.92	0.0006	0.646	0.99
16x16	0.0427	44.40	0.91	0.0005	0.546	0.99

TABLE III  
SPARSITY DISTRIBUTION OF ISGA AND FPC-BB WITH DIFFERENT  $\mu$  VALUES AND PATCH SIZES FOR BARBARA TEST IMAGE

Patch	ISGA				FPC-BB			
	$\mu = 2^{-8}$		$\mu = 2^{-4}$		$\mu = 2^{-8}$		$\mu = 2^{-4}$	
	$m$	$\sigma$	$m$	$\sigma$	$m$	$\sigma$	$m$	$\sigma$
4x4	1.11	1.03	1.11	1.01	1.11	1.05	1.10	1.46
8x8	2.25	4.27	2.25	4.25	2.24	5.50	2.24	5.64
14x14	3.97	11.19	3.92	9.93	3.95	20.67	3.95	18.34
16x16	4.59	11.51	4.63	11.35	4.50	28.96	4.51	26.73

servable sparsity seems to make SDL more robust towards degradations in quality due to variations in important computational parameters such as the patch size. Taking into account the role of the loss terms in the underlying model (4), this appears plausible since the sparsity term may be interpreted as a regularizer that encourages to stick to the main atoms responsible for quality recovery.

## V. CONCLUSION

Our investigation shows that the regime of the sparsity coefficients appears to be ideally visible as a peak around zero in addition to a Gaussian distribution in the histogram of coefficients. The sparsity regime is not only defined by the sparsity parameter in the SDL optimization model, but depends inherently also on the algorithm in use. The observable image reconstruction quality is in general high by the dictionary learning approach, so that a good reconstruction quality does not indicate a low sparsity quality. In turn, high degree of sparsity seems to make SDL more robust against influence of other parameters defining the computational setup.

Let us note again that our investigation relies on the use of histograms of coefficients, which appears to be useful in order to identify and classify sparsity regimes that may be favorable for SDL. In the future we aim to build upon this approach for more detailed assessment of SDL robustness as well as automated parameter choices. We also aim to extend our current scope to denoising and other processes of interest.

Learning-based methods like LISTA (Learned ISTA) [8] and ADMM-Net (Alternating Direction Method of Multipliers-Net) [22] train sparse recovery models with a specific architecture with the aim to produce the best possible approximation of the sparse code and to optimize parameters for the reconstruction task. In future work, we also plan to consider learning models in the sparse coding stage and study possible improvements in accuracy and robustness by learned parameters.

## REFERENCES

- [1] M. Aharon, M. Elad, and A. Bruckstein, "K-SVD: An algorithm for designing overcomplete dictionaries for sparse representation," *IEEE Trans. Signal Process.*, vol. 54, no. 11, pp. 4311–4322, 2006.
- [2] J. M. Bioucas-Dias and M. A. T. Figueiredo, "A new TwIST: Two-step iterative shrinkage/thresholding algorithms for image restoration," *IEEE Trans. Image Process.*, vol. 16, no. 12, pp. 2992–3004, 2007.
- [3] M. Elad, "Sparse and redundant representation from theory to application in signal and image processing," Springer, Berlin, 2010.
- [4] M. Elad and M. Aharon, "Image denoising via sparse and redundant representations over learned dictionaries," *IEEE Trans. Image Process.*, vol. 15, no. 12, pp. 3736–3745, Dec. 2006.
- [5] K. Engan, S. O. Aase, and J. H. Husøy, "Multi-frame compression: Theory and design," *Signal Processing*, vol. 80, no. 10, pp. 2121–2140, 2000.
- [6] H. Esmaeili, S. Shabani, and M. Kimiae, "A new generalized shrinkage conjugate gradient method for sparse recovery," *Calcolo*, vol. 56, no. 1, pp. 1–38, 2019.
- [7] S. Foucart and H. Rauhut, "A mathematical introduction to compressive sensing," Springer, New York 2013.
- [8] K. Gregor and Y. LeCun, "Learning fast approximations of sparse coding," In Proceedings of the 27th international conference on machine learning, pp. 399–406, June 2010.
- [9] R. Giryes and M. Elad, "Sparsity Based Poisson Denoising with Dictionary Learning," *IEEE Trans. Image Process.*, vol. 23, no. 12, pp. 5057–5069, December 2014.
- [10] E. T. Hale, W. Yin, and Y. Zhang, "Fixed-point continuation applied to compressed sensing: implementation and numerical experiments," *J. Comput. Math.*, vol. 28, no. 2, pp. 170–194, 2010. DOI: 10.4208/jcm.2009.10-m1007.
- [11] L. Jing, M. K. Ng, and T. Zeng, "Dictionary learning-based subspace structure identification in spectral clustering," *IEEE Trans. Neural Netw. Learn. Syst.*, vol. 24, no. 8, pp. 1188–1199, Aug. 2013.
- [12] Kaggle dataset. <https://www.kaggle.com/>
- [13] S. Lesage, R. Gribonval, F. Bimbot, and L. Benaroya, "Learning unions of orthonormal bases with thresholded singular value decomposition," *Proc. IEEE Int. Conf. Acoust., Speech, Signal Process. (ICASSP)*, vol. 5, pp. 293–296, 2005.
- [14] M. S. Lewicki and T. J. Sejnowski, "Learning overcomplete representations," *Neural Computation*, vol. 12, no. 2, pp. 337–365, 2000.
- [15] J. Mairal, F. Bach, J. Ponce, and G. Sapiro, "Online dictionary learning for sparse coding," in *Proceedings of the 26th Annual International Conference on Machine Learning (ICML)*, pp. 689–696, 2009.
- [16] L. Ma, L. Moisan, J. Yu, and T. Zeng, "A dictionary learning approach for Poisson image deblurring," *IEEE Trans. Med. Imaging*, vol. 32, no. 7, pp. 1277–1289, July 2013.
- [17] B. A. Olshausen and D. J. Field, "Sparse coding with an overcomplete basis set: A strategy employed by V1?", *Vision Research*, vol. 37, no. 23, pp. 3311–3325, Dec. 1997.
- [18] S. Sardy, A. G. Bruce, and P. Tseng, "Block coordinate relaxation methods for nonparametric wavelet denoising," *J. Comput. Graph. Stat.*, vol. 9, no. 2, pp. 361–379, 2000.
- [19] S. Shabani and M. Breuß, "An efficient line search for sparse reconstruction," in *9th International Conference on Scale Space and Variational Methods in Computer Vision (SSVM)*, LNCS, vol. 14009, Springer, Cham, pp. 471–483, 2023.
- [20] S. Shabani and M. Breuß, "Semi-monotone Goldstein line search strategy with application in sparse recovery," in *Proc. 10th International Conference on Scale Space and Variational Methods in Computer Vision (SSVM)*, LNCS, vol. 15668, Springer, Cham, pp. 69–81, 2025.
- [21] S. Shabani, M. Khoshghaferezaee, and M. Breuß, "Sparse dictionary learning for image recovery by iterative shrinkage," in *IntelliSys 2025*, to appear in *Lecture Notes in Networks and Systems (LNNS)*, Springer. <https://arxiv.org/abs/2503.10732>
- [22] J. Sun, H. Li, and Z. Xu, "Deep ADMM-Net for compressive sensing MRI," *Advances in neural information processing systems*, 29, 2016.
- [23] S. Xiang, G. Meng, Y. Wang, C. Pan, and C. Zhang, "Image deblurring with coupled dictionary learning," *International Journal of Computer Vision*, vol. 114, pp. 248–271, 2015.
- [24] T. Zhang, B. Ghanem, S. Liu, C. Xu, and N. Ahuja, "Low-rank sparse coding for image classification," In *Proceedings of the IEEE international conference on computer vision*, pp. 281–288, 2013.